VOPT: Robust Visual Odometry by Simultaneous Feature Matching and Camera Calibration

Rafael F. V. Saracchini[1], Carlos Catalina[1], Rodrigo Minetto[2] and Jorge Stolfi[3]
[1]Dept. of Simulation and Control, Technological Institute of Castilla y Len, Burgos, Spain
[2]Dept. of Informatics, Federal University of Technology, Paraná, Curitiba, Brazil
[3]Institute of Computing, State University of Campinas, Campinas, Brazil

Keywords: 3D Tracking, Augmented Reality, Camera Calibration, Real-time and GPU Processing.

Abstract: In this paper we describe VOPT, a robust algorithm for visual odometry. It tracks features of the environment with known position in space, which can be acquired through monocular or RGBD SLAM mapping algorithms. The main idea of VOPT is to jointly optimize the matching of feature projections on successive frames, the camera's extrinsic matrix, the photometric correction parameters, and the weight of each feature at the same time, by a multi-scale iterative procedure. VOPT uses GPU acceleration to achieve real-time performance, and includes robust procedures for automatic initialization and recovery, without user intervention. Our tests show that VOPT outperforms the PTAMM algorithm in challenging videos available publicly.

1 INTRODUCTION

Visual odometry (VO) is the determination of the motion of a video camera relative to a static environment by comparing successive video frames (Scaramuzza and Fraundorfer, 2011). This technique is used in several applications in the field of robotics, entertainment and autonomous navigation of terrestrial and aerial vehicles (Weiss et al., 2013). Specifically, it is a core component in most *simultaneous tracking and mapping* (SLAM) algorithms, which acquire a 3D model of the environment as it is traversed. See figure 1.

The contribution of this paper is a robust and efficient algorithm for visual odometry, which we call VOPT, with a GPU-based real-time implementation. The VOPT algorithm uses a sparse model of the environment, consisting of an unstructured collection of salient points in 3-space (optionally with surface normals) that are associated to salient features of the video frames. The positions and normals of those tracked features can be obtained either by multiview stereo or RGBD cameras. Our proposed method also uses local photometric adjustments of individual features to cope with variations in lighting, and is relatively insensitive to motion blur and image noise.

This paper is organized as follows. The environment model and the algorithm are described in Sections 2 and 3. We describe our tests in Section 4 and conclusions in Section 5.

(a) (b)

Figure 1: Input frame and associated visual odometry reference maps: (a) dense depth map and (b) sparse patch map.

1.1 Related Work

Most VO algorithms can be divided in three classes: *feature-based*, *appearance-based* and *patch-based*.

Feature-based algorithms (Concha and Civera, 2014; Castle et al., 2008) identifies a large set of dis-

Saracchini, R., Catalina, C., Minetto, R. and Stolfi, J.
VOPT: Robust Visual Odometry by Simultaneous Feature Matching and Camera Calibration.
DOI: 10.5220/0005781700590066
In *Proceedings of the 11th Joint Conference on Computer Vision, Imaging and Computer Graphics Theory and Applications (VISIGRAPP 2016) - Volume 3: VISAPP*, pages 61-68
ISBN: 978-989-758-175-5

tinguished *features* (such as corners and edges) in a frame, matching them with a reference set and estimating motion accordingly. By computing the positions of features with known 3D position its possible estimate the camera motion position for each captured frame. The most popular algorithm of this class is PTAMM (Castle et al., 2008) and its variants (Klein and Murray, 2009; Weiss et al., 2013). This class of algorithms is relatively insensitive to lighting variations and occlusions. However, the feature detection step is rather costly, since it must allow for affine distortions of the feature's image between frames (Lowe, 2004; Bay et al., 2006; Alcantarilla et al., 2013). Such algorithms are also badly affected by motion blur and noise.

An appearance-based algorithm requires a 3D geometric model of the environment, and tries to determine the camera pose for each frame by minimizing the difference between each observed frame and a rendering of that model with the tentative camera position. This approach was used by the DTAM algorithm of Newcombe *et al*. (Newcombe et al., 2011b) algorithm, which used a dense depth map representation. In order to reduce computational costs, Engel *et al*. (Engel et al., 2013) and Forster *et al*. (Forster et al., 2014) proposed the use of a *semi-dense* model containing only the parts of the depth map near salient elements like edges and corners. These methods are less sensitive to motion blur and noise but are sensitive to lighting variations (although lighting variations can be alleviated by using dense maps (Maxime et al., 2011)).

A patch-based algorithm follows an intermediate approach. It uses a very sparse model of the environment, consisting of a set of flat patches of the environment's surface, with known 3D positions, appearance, and normal vectors. For each frame, the camera position is adjusted until the computed projections of these surface patches match the corresponding parts of the frame image. Examples of this class are the Vachetti *et al*. (Vacchetti et al., 2004), and the AFFTRACK algorithm of Minetto *et al*. (Minetto et al., 2009). These algorithms have lower computational cost than appearance-based algorithms because they don't have to do a full rendering of the environment model for each tentative camera pose; and also lower cost than feature-based algorithms because they can predict the position and deformation of each patch caused by the camera motion. VOPT can use either the feature-based approach or the patch-based approach, depending on the availability of surface data.

2 DATA REPRESENTATION

Video Frames. A video is assumed to be a sequence of N images $\mathcal{F}_0, \mathcal{F}_1, \ldots, \mathcal{F}_{N-1}$, the *frames*, all with n_x columns by n_y rows of pixels. Each frame $\mathcal{F}_i$ can be viewed as a function from the rectangle $\mathcal{D} = [0, n_x] \times [0, n_y]$ of $\mathbb{R}^2$ to some color space, that is derived from the pixel values by some interpolation schema.

Camera Model. We denote by ρ the *projection function* that maps a 3D point p of $\mathcal{C}$ to a 2D point q of $\mathcal{D}$ belong to a frame, where $\mathcal{C} \subset \mathbb{R}^3$ is the cone of visibility of the camera. We assume a pinhole camera model, so that the projection is determined by the 3×4 homogeneous *intrinsic matrix* K of the camera that defines the projection from the camera's coordinate system to the image sensor plane, and by the 4×4 homogeneous *extrinsic matrix* T that defines the current position and pose of the camera relative to the world's coordinate system. We assume K known and radial distortion removed *a priori* and that the camera has fixed focal length (zoom), so that the K matrix is the same for all video frames. We also assume that the video frames have been corrected and do not have any radial distortions.

The projection function ρ is defined by

$$q = \rho_{K,T}(p) = KT^{-1}p \tag{1}$$

where p and q are represented as homogeneous coordinate column vectors. Note that the T matrix includes the 3 coordinates of the camera's position and a 3×3 orthonormal rotation submatrix. We denote by $\vec{v}(T, p)$ the unit direction vector in space from the point $p \in \mathbb{R}^3$ to the position of the camera implied by the extrinsic matrix T and the projection function $\rho_{K,T'}(p)$ which maps a point $p \in \mathbb{R}^3$ into image coordinates.

Tracked Features. The essential information about the environment is a list $S = (s_0, s_1, \ldots, s_{n-1})$ of *features* on its surface. Each feature s_k has a *space position* $s_k.p$ in $\mathbb{R}^3$ and (optionally) a local *surface normal* $s_k.\vec{u} \in \mathbb{S}^2$. (By convention, $s_k.\vec{u}$ is $(0,0,0)$ if the normal is not available.) Each feature s_k is also associated to a sub-image of some reference image $s_k.\mathcal{J}$, called the *canonical projection* of the feature. We will assume that all reference images have the same domain $\mathcal{D}^* = [0, n_x^*] \times [0, n_y^*]$ and were imaged with the same intrinsic camera matrix K^*. The canonical projection of the feature is represented in the algorithm by a pointer to the reference image $s_k.\mathcal{J}$, the extrinsic camera matrix $s_k.T$ already determined for that reference image, a *bounding rectangle* $s_k.R \subset \mathcal{D}^*$, and a *mask* $s_k.\mathcal{M}$. The mask is a pixel array with values in $[0,1]$, spanning that rectangle, that defines the actual

Figure 2: Projection of features s_0 and s_1 on the image $\mathcal{K} = s_0.\mathcal{J} = s_1.\mathcal{J}$, showing their bounding rectangles $s_0.R, s_1.R$ (left) and their masks $s_0.\mathcal{M}, s_1.\mathcal{M}$ (right).

extend and shape of the image feature on the reference image. See figure 2.

Key Frames an Pose Graph. In order to start the tracking, and restart it after a tracking failure, the algorithm requires a list $\mathcal{K} = (\mathcal{K}_0^*, \mathcal{K}_1^*, \ldots, \mathcal{K}_{N^*-1}^*)$ of reference images of the environment, the *key frames*. Specifically, for each key frame $\mathcal{K}_r^* \in \mathcal{K}$, the algorithm requires an extrinsic matrix T_r^* and a set S_r^* of features that are visible in it. It also requires a *pose graph* $\boldsymbol{G}$, whose vertices are the key frames, with an edge between two key frames if their views have sufficient overlap.

This *Key Frame Data* can be obtained from several sources: frame squences, depth maps from with devices like laser rangers and RGBD cameras, structure-from-motion, etc. The feature set and pose graph are then derived from sparse (Castle et al., 2008; Engel et al., 2013) or dense (Newcombe et al., 2011a; Whelan et al., 2012) maps computed by SLAM algorithms. The masks $s_k.\mathcal{M}$ can be determined by back-projecting the bounding rectangle $s_k.R$ into the scene geometry, discarding regions which are not connected to its centre and computing a weight proportional with the difference of the surface normal with $s_k.\vec{u}$. In case of sparse maps, the mask is not computed and all its values are set to 1.

3 TRACKING ALGORITHM

The VOPT algorithm is applied to each frame $I = \mathcal{F}_i$ of a video sequence. Its normal case is described in figure 3. It takes as inputs the collection of tracked space features S, and the previous video frame $I' = \mathcal{F}_{i-1}$ with its extrinsic camera matrix T'. For each feature s_k in S it also receives the *reliability weight* w'_k that measures its visibility in frame I' and how well it matched its canonical projection. If successful, the procedure returns the extrinsic matrix T for frame I, and, for each feature s_k, an adjusted weight w_k. It requires an *startup procedure* (Straub et al., 2013; Saracchini and Ortega, 2014) to select the features S to be tracked on the first image of the video, $I = \mathcal{F}_0$, the extrinsic matrix T_0. We used the approach described in (Saracchini and Ortega, 2014) in order to initialize the system and select the most likely key-frames and associated features from the pose-graph map. This procedure will be briefly described in section 3.3.

Procedure VOPT(S, I, I', T', w') returns (T, w)
1. $(d, w) \leftarrow$ DISPLACEMENTS(S, I', T', w', I)
2. $(T, w) \leftarrow$ ESTIMCAMERA(S, T', d, w);
3. $(T, w) \leftarrow$ CAMADJUST(S, I, T, w)

Figure 3: The normal case of the VOPT algorithm.

The VOPT algorithm can be summarized as follows:
The procedure DISPLACEMENTS in step 1 first computes the position c'_k of each feature pont $s_k.p$ with $w'_k > 0$ on frame I', using the corresponding camera matrix T'. Then it uses the multiscale KLT algorithm of Kanade *et al.* (Shi and Tomasi, 1994) to determine the optical flow $\Phi : \mathcal{D} \to \mathcal{D}$ between the frames I' and I. For efficiency, the flow is computed only in a subset of the domain, consisting of the union of 21×21 pixel squares centred at the points c'_k. The flow Φ is applied to the center $c'_k = \rho_{K,T'}(s_k.p)$ of each feature projection in I' to obtain its approximate apparent position c_k in I. Note that each feature is independently mapped, without considering the constraints of perspective change. The procedure returns the displacement $d_k = c_k - c'_k \in \mathbb{R}^2$ between the projected feature positions on frame I' and their apparent positions on frame I. The weight w_k of each feature is set to zero if $w'_k = 0$, or if any of these steps fails (e.g. if c'_k falls outside $\mathcal{D}$).

In step 2, an initial estimate of the camera matrix T is obtained from the 3D position $s_k.p$ of each feature, the camera matrix T' of the previous frame, and its apparent displacement d_k between the two frames. We use Klein's iterative M-Estimator (Klein, 2006), except that the diagonal weight matrix W is computed by the formula

$$W_{2k,2k} = W_{2k+1,2k+1} = w'_k \left(1 + \frac{r_k}{2}\right)^{-1} \quad (2)$$

where r_k the residual of the computed and observed displacement is the Euclidean length of the difference between the observed displacement d_k and the displacement computed from the 3D position $s_k.p$, the matrix T', and the current version of the matrix T. The M-estimator algorithm usually converges in 10 to 20 iterations. At the end, each reliability weight w_k is updated from the weight matrix W, by inverting formula (2).

In step 3, the initial estimate of the extrinsic matrix T for frame I (wich is often imprecise, due to errors in the displacements d_k) is iteratively refined by the procedure CAMADJUST, simultaneously with the reliability weight w_k for each tracked feature s_k. This step is detailed in section 3.1.

3.1 Camera Pose Refinement

The procedure CAMADJUST receives as input the list S of features that are being tracked, their current weights w_k, the next frame I, and an initial estimate T of its extrinsic matrix. It returns the adjusted matrix T and an updated reliability weight w_k for each feature. The procedure is similar to the core of the AFFTRACK (Minetto et al., 2009). It adjusts the camera matrix T and the reliability weights w_k iteratively for each level l of a image pyramid, by refining the apparent positions the features on the current frame, allowing for differences in illumination between the canonical projection and the current projection of each feature. Features that are not visible eventually get w_k set to zero, and excluded from the computation of T. See figure 4.

Procedure CAMADJUST(S, I, T, w) returns (T, w)
1. Repeat while T does not converge, or until N_{ca} iterations:
    2. For each feature s_k in S,
        3. Let $P_k \leftarrow$ GETLOCALMAP(s_k, T)
        4. $d_k \leftarrow (0,0)$
    5. For each level ℓ from $N_{ms}-1$ down to 0, do
        6. For each feature s_k with a valid map P_k, do
            7. Scale P_k, d_k to level ℓ.
            8. $(d_k, w_k) \leftarrow$ FADJUST$(s_k, P_k, I^{(\ell)}, d_k)$
    9. $(T, w) \leftarrow$ ESTIMCAMERA(s, T, d, w)

Figure 4: The iterative camera adjustment procedure.

Each iteration of CAMADJUST first computes a local 2D projective transformation P_k that describes the estimated position and deformation of each feature s_k from its key frame $s_k.\mathcal{J}$ to the image I, due to camera motion between the two frames, assuming the current guess for the matrix T. Then, for each feature s_k, the procedure determines a displacement d_k from that estimated position to the position that yields the best match with the contents of frame I.This displacement is computed by incremental adjustments at multiple scales of resolution. Finally, the displacements d_k are used to correct the matrix T, by Klein's M-Estimator. The iteration stops when the adjusted matrix T does not change significantly, or after N_{ca} iterations.

Feature Deformation Map. The projective map P_k computed in step 3 is obtained by lifting the rectangle $s_k.R$ to 3D space and projecting it onto the frame I. More precisely, let Π_k be a plane in $\mathbb{R}^3$ that passes through the point $s_k.p$ and is perpendicular to the surface normal $s_k.\vec{u}$. If the surface normal $s_k.\vec{u}$ is not known, then Π is assumed to be perpendicular to $\vec{v}(S, s_k.p)$. Each corner p of the rectangle $s_k.R$ is mapped to a point q of $\mathbb{R}^2$ by

$$q = \rho_{K,T}(\rho^{-1}_{K^*,S,\Pi_k}(p)) \tag{3}$$

where $S = s_k.T$ is the extrinsic matrix of the key frame of that feature, and $\rho^{-1}_{K^*,S,\Pi_k}$ is the function that back-projects that key frame onto the plane Π_k. However,if $s_k.\vec{u} \cdot \vec{v}(T, s_k.p) \leq 0$, or if a corner lies outside $\mathcal{D}$, the feature is considered invisible (self-occluded) in the frame I. and the map P_k is not defined. If the projected corners fall behind the camera or outside $\mathcal{D}$ the feature is considered invisible, and P_k invalid.

Multiscale Processing. In order to achieve robust and efficient discovery of large (multi-pixel) displacements, the feature adjustment step 8 is repeated at multiple scales of resolution, using an image pyramid $I^{(0)} = I$, $I^{(1)}$, $I^{(N_{ms}-1)}$, each level $I^{(\ell)}$ being scaled by $1/2^{\ell}$ in each axis. Note that the weights w_k are recomputed from scratch at each level.

Note also that the map P_k and the accumulated displacement d_k are initially scaled by $1/2^{N_{ms}-1}$ and then scaled by 2 when going from one level to the next finer level. At each level, the FADJUST procedure can only adjust the displacement d_k by a few pixels. However, because of the multiscale processing, the total displacement can be of the order of $2^{N_{ms}-1}$ pixels on the original images.

3.2 Image Feature Position Adjustment

The FADJUST procedure is called for each feature s_k and scale l, to refine the position of the feature on the frame I. The procedure receives a 2D projective map that defines the position and shape of the feature on I, computed from the current guess of the matrix T for that frame; and a displacement d_k found by image matching at coarser scales. First, the procedure estimates the changes in the lighting of the feature between those two frames, then it applies a small correction to the displacement d_k with the Lucas-Kanade local image matching algorithm (Birchfield, 2014). The weight w_k of each feature is defined based on the quality of the match. See figure 5.

Photometric Correction. The procedure PHOTOCORR in step 3 determines the correction of pixel values under lighting effects, which is needed to compensate for changes in illumination

Procedure FADJUST(s_k, P_k, I, d_k) returns (d_k, w_k)
1. Set R_k to the bounding box of $P_k(s_k.R)$ displaced by d_k.
2. If R_k is contained in $\mathcal{D}$ and has at least 4 rows and 4 columns,
   3. $(\alpha_k, \beta_k) \leftarrow$ PHOTOCORR(s_k, P_k, d_k, I)
   4. If $\alpha_k \geq \alpha_{\min}$,
      5. $(d_k, w_k) \leftarrow$ LK($s_k, P_k, d_k, I, \alpha_k, \beta_k$)
   6. else set $w_k \leftarrow 0$
7. else set $w_k \leftarrow 0$

Figure 5: The local feature position adjustment procedure.

between the two frames, including the effects of shadowing, surface orientation, glossy highlights, etc. We assume that these effects can be well approximated by an affine function $I(P_k(p) + d_k) \approx \alpha_k \mathcal{K}(p) + \beta_k$, for any point p within the mask $\mathcal{N} = s_k.\mathcal{M}$; where $\mathcal{K} = s_k.\mathcal{J}$. Basically, α_k is the relative change in contrast, and β_k captures the difference of the 'black levels' of the two images around the respective projections of the feature. The values of α_k and β_k are obtained by weighted least squares, using the squared discrepancy Q defined by

$$Q(d_k, \alpha_k, \beta_k) = \sum_{p \in s'_k.R} \mathcal{N}(p)(\alpha_k \mathcal{K}(p) + \beta_k - I(P_k(p) + d_k))^2 \tag{4}$$

for the given value of the displacement d_k. If α_k is negative (meaning that darker areas of the canonical projection became lighter on the current image, and vice-versa) or zero, the procedure consider the feature lost and/or obscured by pixel noise, setting the weight w_k to zero. On the other hand, β_k can be positive or negative.

Local Feature Matching. In step 5, the Lucas-Kanade (LK) algorithm (Birchfield, 2014) is used to adjust the displacement d_k so that the pixel values of I are most similar to those of $\mathcal{K} = s_k.\mathcal{J}$, after mapped by P_k, displaced by d_k, and color-corrected according to α_k and β_k. The similarity is evaluated by the same Q functional (4) used for photometric correction. If the LK algorithm does not converge after N_{lk} iterations, we consider the adjustment failed, and setting w_k to zero. Otherwise we set w_k to $\exp(-z^2/2)$, where $z = Q/(\alpha_i^2 \sigma^2)$ and σ is the expected standard deviation of the pixel noise.

GPU Acceleration. Steps 3 and 5 of FADJUST are responsible for most of the computational cost of the VOPT algorithm, requiring computation of sums over all pixels of a feature projection, mapped by the deformation map P_k. We compute those sums on GPU by parallel reduction (Harris et al., 2007; Micikevicius, 2009), and warping images by bi-cubic interpolation (Ruijters et al., 2008) using texture memory, which is initialized in the startup procedure. The key frames $s_k.\mathcal{J}$ and the image feature masks $s_k.\mathcal{M}$ are copied into the GPU's texture memory, and the texture warping functions are used to map the pixel positions in the key frame to the current frame by fast cubic interpolation (Ruijters et al., 2008). Those two steps require solving 2×2 linear systems, which are solved in the CPU.

3.3 Initialization and Recovery

The VOPT algorithm requires an auxiliary *startup procedure* to select the features to be tracked on the first image of the video, $I = \mathcal{F}_0$, and to define the extrinsic matrix T_0 for that frame. This procedure is also needed to restart the odometry if the VOPT algorithm fails, e.g. because there are not enough features that are visible in the frame (specifically, if the CAMADJUST procedure ends with fewer than 5 features with non-zero weight w_k). If VOPT fails when trying to go from some frame $I' = \mathcal{F}_{i-1}$ to the next frame $I = \mathcal{F}_i$, we give up on that frame and apply the startup procedure to frame $I = \mathcal{F}_{i+1}$.

The startup procedure looks for the most similar key-frame $\mathcal{K}_r^*$ in $\mathcal{K}$ to the target image I by feature-matching, using the vocabulary tree technique of Nister and Stewenius (Nister and Stewenius, 2006) and extended in (Saracchini and Ortega, 2014). Afterwards, we build a list S of features to be tracked as the union of S_r^* and of all S_s^* such that $\mathcal{K}_s^*$ is adjacent to $\mathcal{K}_r^*$ in the pose graph $\boldsymbol{G}$. The startup procedure then computes an approximate estimate T for the matrix of frame I using RANSAC. Finally it uses the CAMADJUST procedure to improve the estimated camera pose. This procedure, although very robust, is noticeably slower than the odometry procedure due the high computational cost of detecting and matching features.

4 EXPERIMENTS

Test Videos. We tested the VOPT algorithm on both synthetic and real video sequences. See Table 1. In all tests, we set $N_{ca} = 2$, $N_{lk} = 10$ iterations, $N_{ms} = 3$ pyramid levels, $\alpha_{\min} = 0$, and $\sigma = 0.1$. All the algorithms were tested in standard PC with an Intel i5 3.2 Ghz, 4GB of RAM, and Geforce 650 GTX graphics card. The operational system was Linux Debian "wheezy" 64-bit.

The real videos were captured with a hand-held Logitech C930 camera, recording 840×480 frames at 30 fps, with fixed focal length. The intrinsic camera matrix K was determined by OpenCV calibration. One set of real videos (group `M`) was obtained by moving the C930 camera back and forth over a cluttered

Table 1: Video dataset information. Notes: videos with (o) feature occlusion, (m) motion, (l) adverse lighting, (b) motion blur and (*) navigation in unmapped regions.

	Video	Frames	Notes
Synthetic	S0	241	[m]
	S1	241	[o,m]
	S2	241	[b,m]
	S3	241	[o,b,m]
	S4	241	[l,m]
	S5	241	[l,o,m]
	S6	241	[l,b,m]
	S7	241	[l,b,o,m]
Real	M0	711	[o,m]
	M1	510	[o,b,m]
	C0	1207	[o,b,m]
	C1	425	[o,b,m]
	C2	1015	[o]
	C3	709	[o,m]
	C4	666	*[o,b,m]

office desk. Another set of videos (group C) was taken by walking down a laboratory corridor with the camera.

The synthetic videos (group S) were generated by rendering a 3D model of an abbey with the Blender ray-tracer (Blender Online Community, 2014).For each video frame $\mathcal{F}_i$, we saved the corresponding extrinsic camera matrix $T_i^{\#}$ used in the rendering. We selectively enabled challenging factors such as motion blur, localized illumination by spotlights, and occlusion by several objects.

Key Frame Data. For each of the groups S, M, and C, we used the PTAMM (Castle et al., 2008) to obtain one set KPT of key frame data, including the set of key frames $\mathcal{K}$, the pose graph $\boldsymbol{G}$, and, for each key frame $\mathcal{K}_r^*$, the extrinsic matrix T_r^*, and the set of features S_r^* using a reference video without adverse effects. The input to PTAMM was a reference video in plain RGB format, distinct from the test videos. For the M and C groups, the reference video was acquired with the C930 camera. For the S group, the reference video was rendered with Blender, without the extra challenging factors. For each key-frame, we discarded redundant features, accepting at most 60, and a total limit of 180.

We also tested the algorithm with reference maps obtained from depth 3D reconstruction. For the the groups S and C, we produced a set KSO of key frames containing dense data, constructing the pose-graph map with a RGBD-SLAM algorithm (Saracchini and Ortega, 2014) for the C group and by depth-map rendering the 3D model of the abbey at regularly spaced intervals for the S group. The feature sets S_r^* were extracted by using a corner detector (Shi and Tomasi, 1994), discarding regions without depth, and normals computed directly from the depth map.

Algorithms and Metrics. For each test video, we ran the VOPT algorithm with the KPT key frame data set (S, M, and C groups) and with the KSO data set (S and C groups). For comparison, we also ran the visual odometry module of PTAMM (PTAMM-VO) on each video with its original frame data with the key frame data KPT obtained by PTAMM, except that the feature sets were not trimmed. For each test run, we recorded the fraction κ of frames that were successfully calibrated (either by the startup procedure or by VOPT), the number L of tracking losses and average processing time per frame t in milliseconds. For the synthetic videos, we also computed the RMS error $\bar{e}$ between the estimated T_i and the ground-truth $T_i^{\#}$. The test videos, key frame data sets, and outputs of all these runs are available at http://www.liv.ic.unicamp.br/ saracchini/VOPT/.

Results. Our results are summarized in figures 6, 7 and Table 2. It can be seen that VOPT was generally more accurate (smaller $\bar{e}$) and robust (larger κ, smaller L), outperforming PTAMM using less data and achieving best results when using dense data KSO and in both cases it performed much better than PTAMM-VO. The latter failed more often, and had more difficulty in recovery, in the presence of lighting variations, motion blur, and occlusions. It failed only with extreme motion blur or in absence of visible features, which is the case of video C4. VOPT executed in 9–45 ms, depending on the number of iterations needed in steps 2–1 of CAMADJUST and of the Lucas-Kanade step 5 in FADJUST. Recovery after failure was much slower ($50--180$ ms) due the high cost of feature matching. In comparison, PTAMM processed each frame in $8--10$ ms.

5 CONCLUSIONS

Our tests show that the VOPT algorithm is slight slower than PTAMM's visual odometry mode, but is considerably more accurate and robust, especially in the presence of motion blur, occlusions, and localized lighting variations. It owes these qualities mainly to the simultaneous adjustment of the camera matrix, the photometric correction parameters, and the reliability weights of individual features. VOPT was also used with success in indoor navigation algorithms of an assisted living device with on-site AR capabilities (NACODEAL, 2014).

Besides its robustness, the proposed algorithm still have limitations which shall be overcome in future works. Namely, it depends on an associated SLAM method to compute the features data needed

Table 2: Tests with computed values of L (tracking losses), κ (successfully calibration), $\bar{e}$ (RMS error) and t (time in ms).

Video	VOPT (sparse - KPT)				VOPT (dense - KSO)				PTAMM-VO			
	L	κ	$\bar{e}$	t	L	κ	$\bar{e}$	t	L	κ	$\bar{e}$	t
S0	0	1.00	0.048	16.9	0	1.00	0.008	18.8	0	0.98	0.042	3.4
S1	0	1.00	0.049	18.6	0	1.00	0.008	20.9	0	0.98	0.043	3.2
S2	0	1.00	0.062	17.2	0	1.00	0.055	19.5	1	0.85	1.002	2.9
S3	0	1.00	0.061	19.2	0	1.00	0.082	21.6	1	0.84	0.732	2.8
S4	0	1.00	0.042	18.9	0	1.00	0.009	22.1	3	0.79	7.679	1.9
S5	0	1.00	0.037	19.6	0	1.00	0.012	23.1	3	0.48	2.897	3.0
S6	0	1.00	0.060	20.2	0	1.00	0.046	25.1	2	0.11	1.507	1.2
S7	0	1.00	0.064	20.7	0	1.00	0.051	24.8	2	0.14	4.774	1.1
M0	0	1.00	-	27.3	-	-	-	-	6	0.92	-	2.1
M1	0	1.00	-	30.7	-	-	-	-	13	0.67	-	3.1
C0	2	0.99	-	15.2	0	1.00	-	15.5	10	0.52	-	1.8
C1	1	0.97	-	14.9	0	1.00	-	18.8	2	0.88	-	2.0
C2	0	1.00	-	12.3	0	1.00	-	14.6	4	0.79	-	2.1
C3	0	1.00	-	13.5	0	1.00	-	16.4	3	0.81	-	1.7
C4	9	0.83	-	12.8	11	0.87	-	18.7	11	0.71	-	2.3

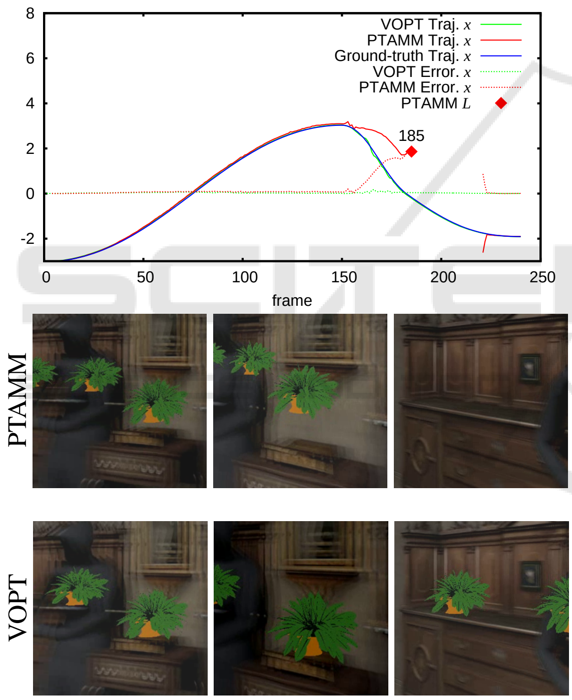

(a) S3-165 (b) S3-173 (c) S3-185

Figure 6: Plot of x camera position of sequence S3, and AR output in the virtual scene with its respective sequence and frames. Note the increasing drift in the AR output of PTAMM.

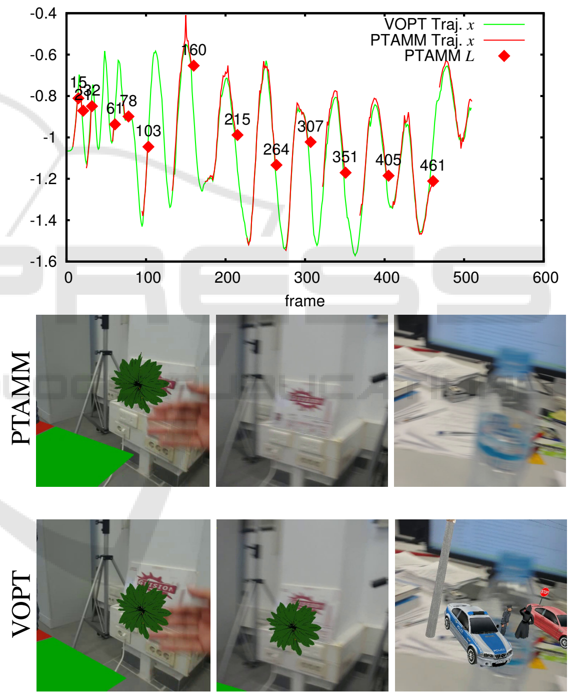

(a) C0-794 (b) C3-287 (c) M1-354

Figure 7: Plot of x camera position of sequence M1, and AR output (plant/car) in occurrence of occlusions(a), motion blur(b) and both conditions(c) with its respective sequence and frames.

for odometry. It also do not provide an efficient method to update the list of tracked features from the map after initialization. In the current implementation it allows to local tracking only, if the camera moves outside the region covered by the selected patches a tracking loss and subsequent reinitialization will follow. Finally the dependency on a GPU makes it less suitable for devices without a dedicated graphics card.

Future works will involve the development of light-weight version of VOPT aimed to mobile devices, as well the incorporation of the VOPT as effective module of a full SLAM system, overcoming the aforementioned limitations. We aim also for a more efficient usage of the GPU capabilities by exploiting cache and spatial locality.

ACKNOWLEDGEMENTS

This work was funded by the Ambient Assisted Living Joint Programme as part of the project Natural Communication Device for Assisted Living, ref. AAL-2010-3-116 (NACODEAL, 2014).

REFERENCES

Alcantarilla, P. F., Nuevo, J., and Bartoli, A. (2013). Fast explicit diffusion for accelerated features in nonlinear scale spaces. In *British Machine Vision Conf. (BMVC)*.

Bay, H., Tuytelaars, T., and Van Gool, L. (2006). Surf: Speeded up robust features. In Leonardis, A., Bischof, H., and Pinz, A., editors, *Computer Vision – ECCV 2006*, volume 3951 of *Lecture Notes in Computer Science*, pages 404–417. Springer Berlin / Heidelberg.

Birchfield, S. (2014). Derivation of kanade-lucas-tomasi tracking equation. https://www.ces.clemson.edu/ stb/klt/birchfield-klt-derivation.pdf.

Blender Online Community (2014). *Blender - a 3D modelling and rendering package*. Amsterdam.

Castle, R., Klein, G., and Murray, D. (2008). Video-Rate Localization in Multiple Maps for Wearable Augmented Reality. In *IEEE International Symposium on Wearable Computers (ISWC)*, pages 15–22.

Concha, A. and Civera, J. (2014). Using Superpixels in Monocular SLAM. In *IEEE International Conference on Robotics and Automation (ICRA)*, pages 365–372.

Engel, J., Sturm, J., and Cremers, D. (2013). Semi-dense visual odometry for a monocular camera. In *IEEE International Conference on Computer Vision (ICCV)*, pages 1449–1456.

Forster, C., Pizzoli, M., and Scaramuzza, D. (2014). SVO: Fast Semi-Direct Monocular Visual Odometry. In *IEEE International Conference on Robotics and Automation (ICRA)*, pages 15–22.

Harris, M. et al. (2007). Optimizing Parallel Reduction in CUDA. *NVIDIA Developer Technology*, 2(4).

Klein, G. (2006). *Visual Tracking for Augmented Reality*. PhD thesis, University of Cambridge.

Klein, G. and Murray, D. (2009). Parallel tracking and mapping on a camera phone. In *IEEE International Symposium on Mixed and Augmented Reality (ISMAR)*, pages 83–86.

Lowe, D. G. (2004). Distinctive image features from scale-invariant keypoints. *Int. J. Comput. Vision*, 60(2):91–110.

Maxime, M., Comport, A., and Rives, P. (2011). Real-Time Dense Visual Tracking under Large Lighting Variations. In *British Machine Vision Conference (BMVC)*, pages 45.1–45.11. BMVA Press.

Micikevicius, P. (2009). 3D Finite Difference Computation on GPUs using CUDA. In *Workshop on General Purpose Processing on Graphics Processing Units*, pages 79–84. ACM.

Minetto, R., Leite, N., and Stolfi, J. (2009). AFFTrack: Robust Tracking of Features in Variable-Zoom Videos. In *IEEE International Conference on Image Processing (ICIP)*, pages 4285–4288.

NACODEAL (2014). NACODEAL - Natural Communication Device for Assisted Living. European Union Project. www.nacodeal.eu. Ambient Assisted Living Joint Programme ref. AAL-2010-3-116.

Newcombe, R., Izadi, S., Hillige, O., Molyneaux, D., Kim, D., Davison, A., Kohli, P., Shotton, J., Hodges, S., and Fitzgibbon, A. (2011a). KinectFusion: Real-time Dense Surface Mapping and Tracking. In *IEEE International Symposium on Mixed and Augmented Reality (ISMAR)*, pages 127–136.

Newcombe, R., Lovegrove, S., and Davison, A. (2011b). DTAM: Dense Tracking and Mapping in Real-Time. In *IEEE International Conference on Computer Vision (ICCV)*, pages 2320–2327.

Nister, D. and Stewenius, H. (2006). Scalable recognition with a vocabulary tree. In *IEEE Computer Society Conference on Computer Vision and Pattern Recognition*, volume 2, pages 2161–2168.

Ruijters, D., Romeny, B., and Suetens, P. (2008). Efficient GPU-Based Texture Interpolation using Uniform B-Splines. *Journal of Graphics, GPU, and Game Tools*, 13(4):6169.

Saracchini, R. and Ortega, C. (2014). An Easy to Use Mobile Augmented Reality Platform for Assisted Living using Pico-projectors. In *Computer Vision and Graphics*, volume 8671 of *Lecture Notes in Computer Science*, pages 552–561. Springer.

Scaramuzza, D. and Fraundorfer, F. (2011). Visual odometry [tutorial]. *Robotics & Automation Magazine, IEEE*, 18(4):80–92.

Shi, J. and Tomasi, C. (1994). Good Features to Track. In *IEEE Conference on Computer Vision and Pattern Recognition (CVPR)*, pages 593–600.

Straub, J., Hilsenbeck, S., Schroth, G., Huitl, R., Moller, A., and Steinbach, E. (2013). Fast Relocalization for Visual Odometry using Binary Features. In *IEEE International Conference on Image Processing (ICIP)*, pages 2548–2552.

Vacchetti, L., Lepetit, V., and Fua, P. (2004). Stable Real-Time 3D Tracking Using Online and Offline Information. *IEEE Trans. Pattern Anal. Mach. Intell.*, 26(10):1385–1391.

Weiss, S., Achtelik, M., Lynen, S., Achtelik, M., Kneip, L., Chli, M., and Siegwart, R. (2013). Monocular Vision for Long-term Micro Aerial Vehicle State Estimation: A Compendium. *Journal of Field Robotics*, 30(5):803–831.

Whelan, T., Kaess, M., Fallon, M., Johannsson, H., Leonard, J., and McDonald, J. (2012). Kintinuous: Spatially Extended KinectFusion. Technical Report MIT-CSAIL-TR-2012-020, MIT.